QUARTERLY JOURNAL OF THE ROYAL METEOROLOGICAL SOCIETY
Q. J. R. Meteorol. Soc. **133**: 251–260 (2007)
Published online in Wiley InterScience
(www.interscience.wiley.com) DOI: 10.1002/qj.11

The remapped particle-mesh semi-Lagrangian advection scheme

C. J. Cotter,[a] J. Frank[b] and S. Reich[c]*
[a] *Imperial College London, United Kingdom*
[b] *CWI Amsterdam, The Netherlands*
[c] *Universität Potsdam, Germany*

ABSTRACT: We describe the remapped particle-mesh advection method, a new mass-conserving method for solving the density equation which is suitable for combining with semi-Lagrangian methods for compressible flow applied to numerical weather prediction. In addition to the conservation property, the remapped particle-mesh method is computationally efficient and at least as accurate as current semi-Lagrangian methods based on cubic interpolation. We provide results of tests of the method in the plane, results from incorporating the advection method into a semi-Lagrangian method for the rotating shallow-water equations in planar geometry, and results from extending the method to the surface of a sphere. Copyright © 2007 Royal Meteorological Society

KEY WORDS semi-Lagrangian advection; mass conservation; particle-mesh method; spline interpolation

Received 21 June 2006; Revised 5 October 2006; Accepted 2 November 2006

1. Introduction

The semi-implicit semi-Lagrangian (SISL) method, as originally introduced by Robert (1982), has become very popular in numerical weather prediction (NWP). The semi-Lagrangian aspect of SISL schemes allows for a relatively accurate treatment of advection while at the same time avoiding step size restrictions of explicit Eulerian methods. The standard semi-Lagrangian algorithm (see, e.g. Staniforth and Coté, 1991) calculates departure points, i.e. the positions of Lagrangian particles which will be advected onto the grid during the time step. The momentum and density equations are then solved along the trajectory of the particles. This calculation requires interpolation to obtain velocity and density values at the departure point. It has been found that cubic Lagrangian and cubic spline interpolation are both accurate and computationally tractable (see, e.g. Staniforth and Coté, 1991).

Ideally, as well as being efficient and accurate, a density advection scheme should exactly preserve mass in order to be useful for, e.g. climate prediction or atmospheric chemistry calculations. Recent developments have involved computing the change in volume elements, defined between departure and arrival points, making use of a technique called cascade interpolation (Purser and Leslie, 1991). Several such methods have been suggested in recent years, including the methods of Nair and Machenhauer (2002); Nair *et al.* (2002); Nair *et al.* (2003) and the SLICE schemes of Zerroukat *et al.* (2002); Zerroukat *et al.* (2004); Zerroukat *et al.* (2006a); Zerroukat *et al.* (2006b).

In this paper, we give a new density advection scheme, the remapped particle-mesh method, which is based on the particle-mesh discretization for the density equation used in the Hamiltonian Particle-Mesh (HPM) method suggested by Frank *et al.* (2002), which itself is a combination of smoothed particle-hydrodynamics (Lucy, 1977; Gingold and Monaghan, 1977) and particle-in-cell methods (Harlow, 1964). The particle-mesh method provides a very simple discretization which conserves mass by construction, and may be adapted to nonplanar geometries such as the sphere (Frank and Reich, 2004). In this paper, we show that an efficient scheme can be obtained by mapping the particles back to the grid after each time step. Our numerical results show that this scheme is of comparable accuracy to other mass-conserving semi-Lagrangian advection schemes. We show how the method may be included in the staggered semi-Lagrangian schemes, proposed by Staniforth *et al.* (2006) and Reich (2006), and show how to adapt it to spherical geometry.

In section 2, we describe the particle-mesh discretization for the density equation. The method is modified to form the remapped particle-mesh method in section 3. We discuss issues of efficient implementation in section 4 and an extension to spherical geometry in section 5. In section 6, we give numerical results for advection tests in planar geometry and on the sphere, as well as results from rotating shallow-water simulations using the remapped particle-mesh method in the staggered leapfrog scheme

* Correspondence to: S. Reich, Universität Potsdam, Institut für Mathematik, Postfach 60 15 53, D-14415 Potsdam, Germany.
E-mail: sreich@math.uni-potsdam.de

(Reich, 2006). We give a summary of our results and discussion in section 7.

2. Continuity equation and particle advection

This section describes the particle-mesh discretization for the density equation. This discretization forms the basis for the remapped particle-mesh method discussed in this paper. For simplicity, the discussion is restricted to two-dimensional flows.

The discussion begins with the continuity equation

$$\rho_t + \nabla \cdot (\rho \mathbf{u}) = 0, \tag{1}$$

where ρ is the density and $\mathbf{u} = (u, v)^T \in \mathbb{R}^2$ is the fluid velocity. Writing (1) in the Lagrangian formulation as

$$\frac{D\mathbf{X}}{Dt} = \mathbf{u}, \tag{2}$$

$$\rho(\mathbf{x}, t) = \int \rho^0(\mathbf{x}^0)\, \delta(\mathbf{x} - \mathbf{X}(\mathbf{x}^0, t))\, \mathrm{d}A(\mathbf{x}^0), \tag{3}$$

where $\delta(\cdot)$ denotes the Dirac delta function, $\mathrm{d}A(\mathbf{x}^0)$ denotes the infinitesimal area element at $\mathbf{x}^0 = (x^0, y^0)^T \in \mathbb{R}^2$, $\rho(\mathbf{x}, t)$ is the density at time $t \geq 0$ at a fixed Eulerian position $\mathbf{x} = (x, y)^T \in \mathbb{R}^2$,

$$\frac{D}{Dt}(\cdot) = (\cdot)_t + (\cdot)_x\, u + (\cdot)_y\, v \tag{4}$$

is the Lagrangian time derivative,

$$\mathbf{X}(\mathbf{x}^0, t) = (X(\mathbf{x}^0, t), Y(\mathbf{x}^0, t))^T \in \mathbb{R}^2 \tag{5}$$

is a Lagrangian particle position at time t with initial position $\mathbf{X}(\mathbf{x}^0, 0) = \mathbf{x}^0 \in \mathbb{R}^2$, and $\rho^0(\mathbf{x}) = \rho(\mathbf{x}, 0)$ is the initial density.

To discretize the integral representation (3), a finite set of Lagrangian particles $\mathbf{X}_\beta(t) = (X_\beta(t), Y_\beta(t))^T \in \mathbb{R}^2$, $\beta = 1, \ldots, N$, and a fixed Eulerian grid $\mathbf{x}_{k,l} = (x_k, y_l)^T = (k \cdot \Delta x, l \cdot \Delta y)^T$, $k, l = 0, \ldots, M$ are introduced. The Eulerian grid density $\rho_{k,l}(t) \approx \rho(\mathbf{x}_{k,l}, t)$ is then approximated by

$$\rho_{k,l}(t) := \sum_\beta \rho^0(\mathbf{x}^0_\beta)\, \psi_{k,l}(\mathbf{X}_\beta(t))\, A_\beta, \tag{6}$$

where $\psi_{k,l}(\mathbf{x}) \geq 0$ are basis functions, which satisfy $\int \psi_{k,l}(\mathbf{x})\, \mathrm{d}A(\mathbf{x}) = 1$. The particles are initially arranged on a uniform grid with grid cell areas denoted by A_β. Equation (6) may be simplified to

$$\rho_{k,l}(t) = \sum_\beta m^0_\beta\, \psi_{k,l}(\mathbf{X}_\beta(t)), \tag{7}$$

where $m^0_\beta := \rho^0_\beta\, A_\beta$ is the 'mass' of particle β and $\rho^0_\beta := \rho^0(\mathbf{x}^0_\beta)$.

Let the basis functions ψ_{kl} satisfy the partition-of-unity (PoU) property

$$\sum_{k,l} \psi_{k,l}(\mathbf{x})\, A_{k,l} = 1, \qquad A_{k,l} := \Delta x \Delta y, \tag{8}$$

for all $\mathbf{x} \in \mathbb{R}^2$. This ensures that the total mass is conserved since

$$\sum_{k,l} \rho_{k,l}(t)\, A_{k,l} = \sum_{k,l} \sum_\beta m^0_\beta\, \psi_{k,l}(\mathbf{X}_\beta(t))\, A_{k,l} = \sum_\beta m^0_\beta, \tag{9}$$

which is constant. The time evolution of the particle positions $\mathbf{X}_\beta(t)$ is simply given by

$$\frac{d}{dt}\mathbf{X}_\beta = \mathbf{u}_\beta. \tag{10}$$

Given a time-dependent (Eulerian) velocity field $\mathbf{u}(\mathbf{x}, t)$, (7) and (10) can be discretized in time with a simple differencing method:

$$\mathbf{X}^{n+1}_\beta = \mathbf{X}^n_\beta + \Delta t \mathbf{u}^{n+1/2}_\beta, \quad \mathbf{u}^{n+1/2}_\beta := \mathbf{u}(\mathbf{X}^n_\beta, t_{n+1/2}), \tag{11}$$

$$\rho^{n+1}_{k,l} = \sum_\beta^n m^0_\beta\, \psi_{k,l}(\mathbf{X}^{n+1}_\beta). \tag{12}$$

In Frank *et al.* (2002), this discretization was combined with a time stepping method for the momentum equation to form a Hamiltonian particle-mesh method for the rotating shallow-water equations. The masses m^0_β were kept constant throughout the simulation. The HPM advection scheme is somewhat similar to the Lagrangian advection scheme, as proposed by Kaas *et al.* (1997), using tracer points.

In this paper, the HPM discretization is instead combined with a remapping technique so that the particles' trajectories start from grid points at the beginning of each time step. Similar to other mass-conserving advection schemes, this remapping approach requires the assignment of new particle 'masses' in each time step. Contrary to the volume-based (finite-volume type) remapping strategy of, for example, Nair and Machenhauer (2002), mass-parcels are assigned to each grid point, which are moved downstream to provide the density approximation as a superposition of these parcels. This approximation can be implemented very efficiently. The resulting remapping conserves mass globally but not locally (in contrast to volume-based remapping methods). A related downstream advection scheme has been proposed by Laprise and Plante (1995). However, the definition of mass-parcels and the assignment of mass is fundamentally different.

3. Remapped particle-mesh method

This section describes the remapped particle-mesh method for solving the continuity equation. The aim is to exploit the mass conservation property of the

DOI: 10.1002/qj

particle-mesh method whilst keeping an Eulerian grid data structure for velocity updates. To achieve this the particles are reset to an Eulerian grid point at the beginning of each time step, i.e.

$$\mathbf{X}_\beta^n = \mathbf{x}_\beta^n := \mathbf{x}_{k,l}, \qquad \beta = 1 + k + l \cdot (M+1). \quad (13)$$

This step requires the calculation of new particle 'masses' m_β^n, $\beta = 1, \ldots, N$, according to

$$\rho_{k,l}^n = \sum_\beta m_\beta^n \, \psi_{k,l}(\mathbf{x}_\beta^n) \quad (14)$$

for given densities $\rho_{k,l}^n$. This is the remapping step. Finally the particles are stepped forward and the new density on the Eulerian grid is calculated using equations (11) and (12) with m_β^0 being replaced by m_β^n. Note that the Lagrangian trajectory calculation (11) can be replaced by any other consistent forward trajectory approximation. Exact trajectories for a given time-independent velocity field $\mathbf{u}(\mathbf{x})$ will, for example, be used in the numerical experiments.

The whole process is mass conserving since the PoU property (8) ensures that

$$\begin{aligned} \sum_\beta m_\beta^n &= \sum_{k,l} \sum_\beta m_\beta^n \, \psi_{k,l}(\mathbf{X}_\beta^{n+1}) A_{k,l} \\ &= \sum_{k,l} \rho_{k,l}^{n+1} \, A_{k,l} = \sum_\beta m_\beta^{n+1}. \end{aligned} \quad (15)$$

4. Efficient implementation

This density advection scheme can be made efficient since all the interpolation takes place on the grid; this means that the same linear system of equations, characterized by (14), is solved at each time step. The particle trajectories are uncoupled and thus may even be calculated in parallel.

The computation of the particle masses in (14) leads to the solution of a sparse matrix system. This issue is discussed in detail for (area-weighted) tensor product cubic B-spline basis functions, defined by

$$\psi_{k,l}(\mathbf{x}) := \frac{1}{\Delta x \Delta y} \, \psi_{\mathrm{cs}}\left(\frac{x - x_k}{\Delta x}\right) \cdot \psi_{\mathrm{cs}}\left(\frac{y - y_l}{\Delta y}\right), \quad (16)$$

where $\psi_{\mathrm{cs}}(r)$ is the cubic B-spline

$$\psi_{\mathrm{cs}}(r) = \begin{cases} \frac{2}{3} - |r|^2 + \frac{1}{2}|r|^3, & |r| \le 1, \\ \frac{1}{6}(2 - |r|)^3, & 1 < |r| \le 2, \\ 0, & |r| > 2. \end{cases} \quad (17)$$

The basis functions satisfy

$$\sum_{k,l} \psi_{k,l}(\mathbf{x}) \, A_{k,l} = 1 \quad (18)$$

and

$$\int \psi_{k,l}(\mathbf{x}) \, \mathrm{d}A(\mathbf{x}) = 1 \quad (19)$$

as required.

A few basic manipulations reveal that (14) becomes equivalent to

$$\begin{aligned} \rho_{k,l}^n \, A_{kl} &= \rho_{k,l}^n \, \Delta x \Delta y \\ &= \left(1 + \frac{\Delta x^2}{6} \delta_x^2\right) \left(1 + \frac{\Delta y^2}{6} \delta_y^2\right) m_{k,l}^n \end{aligned} \quad (20)$$

where

$$\begin{aligned} \delta_x^2 \, m_{k,l}^n &= \frac{m_{k+1,l}^n - 2m_{k,l}^n + m_{k-1,l}^n}{\Delta x^2}, \\ \delta_y^2 \, m_{k,l}^n &= \frac{m_{k,l+1}^n - 2m_{k,l}^n + m_{k,l-1}^n}{\Delta y^2}, \end{aligned} \quad (21)$$

are the standard second-order central difference approximations, and replacing index $\beta = 1 + k + l \cdot (M+1)$ by k, l, i.e. writing $m_{k,l}^n$, $\mathbf{X}_{k,l}^n$, etc. from now on. Equation (20) implies that the particle masses can be found by solving a tridiagonal system along each grid line (in each direction).

It is instructive to compute the response function for (20), i.e. to evaluate the resulting masses $m_{k,l}^n$ for a density $\rho_{k,l}^n$ that is concentrated at a single grid point. The response function for $\Delta x = \Delta y = 1$ can be found in Figure 1. It can be seen that the resulting values for $m_{k,l}^n$ are non-zero in an extended neighborhood and some values are even negative. The implication is that the cubic B-spline approach does not satisfy strict local mass-conservation, can potentially lead to negative masses, and does not preserve monotonicity. Negative masses can be avoided by a local redistribution of mass values (such that total mass is conserved). At present it is not clear

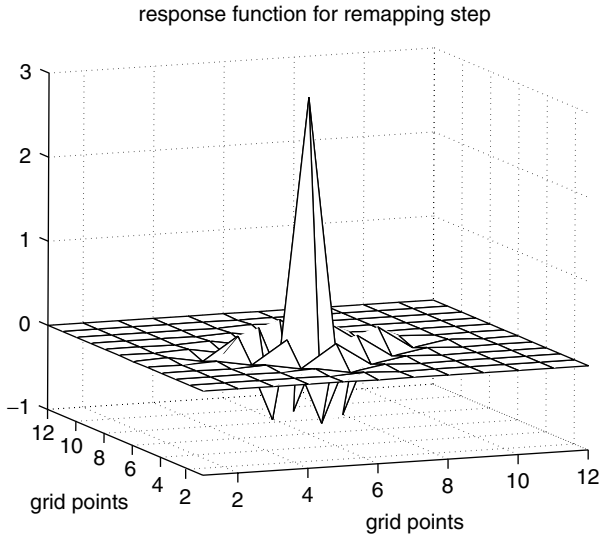

Figure 1. Resulting mass values $m_{k,l}$ for a density $\rho_{k,l}$ concentrated at a single grid point. The mesh-size is $\Delta x = \Delta y = 1$.

DOI: 10.1002/qj

how to preserve strict monotonicity under cubic B-spline interpolation in a systematic manner.

If the cubic spline $\psi_{\rm cs}$ in (16) is replaced by the linear spline

$$\psi_{\rm ls}(r) = \begin{cases} 1-|r|, & |r| \le 1, \\ 0, & |r| > 1, \end{cases} \tag{22}$$

then the system (14) is solved by

$$m^n_{k,l} = \Delta x \Delta y \, \rho^n_{k,l}. \tag{23}$$

The resulting low-order advection scheme possesses the desirable property that $\rho^n_{k,l} \ge 0$ for all k, l implies that $\rho^{n+1}_{k,l} \ge 0$ for all k, l. Local conservation of mass, in the sense of finite-volume methods, and monotonicity are now also achieved. In general, a remapping with linear splines can lead to undesirable levels of numerical diffusion. However, implementations for the rotating shallow-water equations in planar geometry give encouraging results. See the numerical results in section 6. It should also be noted that it is not necessary to remap the particles to a grid position after each single time step as long as the particles keep a relative uniform distribution.

On a more abstract level, conservative advection schemes can be derived for general (e.g. triangular) meshes with basis functions $\phi_{kl}(\mathbf{x}) \ge 0$, which form a partition of unity. An appropriate quadrature formula for (3) leads then to a discrete approximation of type (7). This extension will be the subject of a forthcoming publication.

5. Extension to the sphere

In this section we suggest a possible implementation of the remapped particle-mesh method for the density equation on the sphere. The method follows the particle-mesh discretization given by Frank and Reich (2004), combined with a remapping to the grid.

A longitude-latitude grid with equal grid spacing $\Delta\lambda = \Delta\theta = \pi/J$ is introduced. The latitude grid points are offset a half-grid length from the poles. Hence grid points (λ_k, θ_l) are obtained, where $\lambda_k = k\Delta\lambda$, $\theta_l = -\frac{\pi}{2} + (l-1/2)\Delta\theta$, $k = 1, \ldots, 2J$, $l = 1, \ldots, J$, and the grid dimension is $2J \times J$.

Let $\psi_{k,l}(\mathbf{x})$ denote the (area-weighted) tensor product cubic B-spline centred at a grid point $\mathbf{x}_{kl} \in \mathbb{R}^3$ with longitude-latitude coordinates (λ_k, θ_l), *i.e.*

$$\psi_{k,l}(\mathbf{x}) := \frac{1}{A_{k,l}} \psi_{\rm cs}\left(\frac{\lambda - \lambda_k}{\Delta\lambda}\right) \cdot \psi_{\rm cs}\left(\frac{\theta - \theta_l}{\Delta\theta}\right), \tag{24}$$

where (λ, θ) are the spherical coordinates of a point $\mathbf{x} = (x, y, z)^T \in \mathbb{R}^3$ on the sphere, $\psi_{\rm cs}(r)$ is the cubic B-spline as before, and

$$A_{k,l} := R^2 \cos(\theta_l)\, \Delta\theta \Delta\lambda. \tag{25}$$

Conversion between Cartesian and spherical coordinates is performed using the formulas

$$x = R\cos\lambda\, \cos\theta, \quad y = R\sin\lambda\, \cos\theta, \quad z = R\sin\theta, \tag{26}$$

and

$$\lambda = \tan^{-1}\left(\frac{y}{x}\right), \qquad \theta = \sin^{-1}\left(\frac{z}{R}\right). \tag{27}$$

At each time step the fluid velocity is written in 3D Cartesian coordinates and the particles $\mathbf{X}_{i,j}$ are stepped forward. The particle positions are then projected onto the surface of the sphere as described by Frank and Reich (2004). The Lagrangian trajectory algorithm is then:

$$\mathbf{X}^{n+1}_{i,j} = \mathbf{x}_{i,j} + \Delta t \mathbf{u}^{n+1/2}_{i,j} + \mu\, \mathbf{x}_{i,j}, \tag{28}$$

where μ is a Lagrange multiplier chosen so that $\|\mathbf{X}^{n+1}_{i,j}\| = R$ on a sphere of radius R. This algorithm can be replaced by any other consistent forward trajectory approximation. Exact trajectories are, for example, used in the numerical experiments.

The particle masses $m^n_{i,j}$ are computed by solving the system

$$\rho^n_{k,l} = \sum_{i,j} m^n_{i,j}\, \psi_{k,l}(\mathbf{x}_{i,j}) \tag{29}$$

for given densities $\rho^n_{k,l}$. The density at time-level t_{n+1} is then determined by

$$\rho^{n+1}_{k,l} = \sum_{i,j} m^n_{i,j}\, \psi_{k,l}(\mathbf{X}^{n+1}_{i,j}). \tag{30}$$

Note that the system (29) is equivalent to

$$\rho^n_{k,l}\, A_{k,l} = \left(1 + \frac{\Delta\lambda^2}{6}\delta^2_\lambda\right)\left(1 + \frac{\Delta\theta^2}{6}\delta^2_\theta\right) m^n_{k,l} \tag{31}$$

and can be solved efficiently as outlined in section 4. The implementation of the remapping method is greatly simplified by making use of the periodicity of the spherical coordinate system in the following sense. The periodicity is trivial in the longitudinal direction. For the latitude, a great circle meridian is formed by connecting the latitude data separated by an angular distance π in longitude (or J grid points). See, for example, the paper by Spotz *et al.* (1998). It is then efficient to solve the system (31) using a direct solver.

Conservation of mass is encoded in

$$\sum_{k,l} \rho^{n+1}_{k,l}\, A_{k,l} = \sum_{k,l} \rho^n_{k,l}\, A_{k,l}, \tag{32}$$

which holds because of the PoU property

$$\sum_{k,l} \psi_{kl}(\mathbf{x})\, A_{k,l} = 1. \tag{33}$$

DOI: 10.1002/qj

6. Numerical results

6.1. 1D convergence test

Following Zerroukat *et al.* (2006a), the convergence rate of our method for one-dimensional uniform advection of a sine wave over a periodic domain $\Omega = [0, 1)$ is tested. The initial distribution is

$$\rho_0(x) = \sin(2\pi x) \tag{34}$$

and the velocity field is $u(x, t) = U = 1$. The 1D version of our method is used to solve the continuity equation

$$\rho_t = -(\rho u)_x. \tag{35}$$

The experimental setting is equivalent to that of Zerroukat *et al.* (2006a). Table I displays the convergence of l_2 errors as a function of resolution $\Delta x = 1/M$. Note that the results from Table I are in exact agreement with those displayed in Table I of Zerroukat *et al.* (2006a) for the parabolic spline method (PSM) and fourth-order accuracy is observed. The observed equivalence between our remapped particle-mesh advection scheme and PSM only holds for one-dimensional uniform advection. In particular, the extension to multi-dimensions (Zerroukat *et al.*, 2006b) is fundamentally different.

6.2. 2D planar advection: Slotted-cylinder problem

The slotted-cylinder problem consists of a solid-body rotation of a slotted cylinder in a flow field that rotates with constant angular velocity about a fixed point. The slotted-cylinder problem as, for example, described in Nair *et al.* (1999a); Zerroukat *et al.* (2002) was implemented.

Results for the newly proposed advection scheme can be found in Figure 2. The root-mean-square (rms) difference between the pointwise (rms_1) and the grid-box-averaged (rms_2) analytic solution and the numerical one as well as the relative error in total mass (pdm) were calculated. See Zerroukat *et al.* (2002) for a precise definition of these error measures. It is found that the rms values for our method are slightly smaller than those reported in Zerroukat *et al.* (2002).

6.3. 2D planar advection: Idealized cyclogenesis problem

The idealized cyclogenesis problem (see, e.g. Nair *et al.* (1999a); Zerroukat *et al.* (2002)) consists of a circular vortex with a tangential velocity $V(r) = v_0 \tanh(r)/\text{sech}^2(r)$, where r is the radial distance from the centre

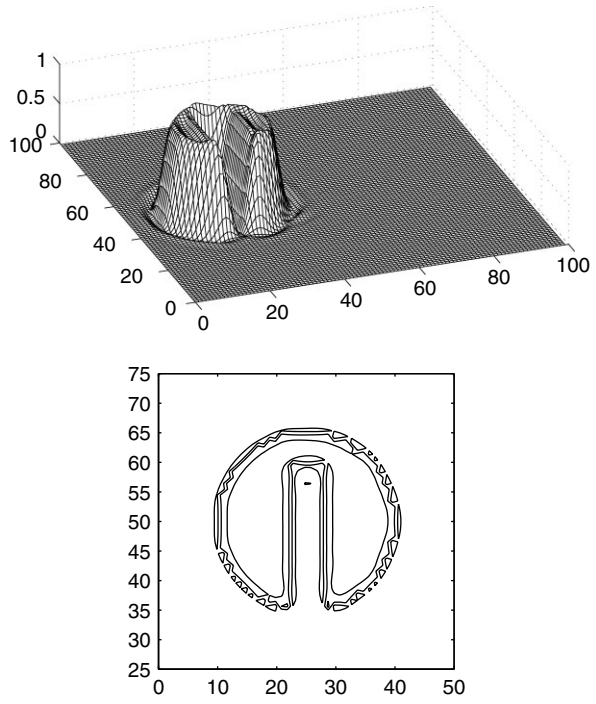

Figure 2. Rotating slotted-cylinder problem. Top panel: numerical solution after six rotations. Bottom panel: error (analytic minus numerical) with contour minimum −0.5266 and contour interval 0.3803; error measures, as defined in Zerroukat *et al.* (2002), $\text{rms}_1 = 0.062595$, $\text{rms}_2 = 0.037329$, and $\text{pdm} = 1.454 \times 10^{-11}$.

of the vortex (x_c, y_c) and v_0 is a constant chosen such that the maximum value of $V(r)$ is unity. The analytic solution $\rho(\mathbf{x}, t)$ is

$$\rho(\mathbf{x}, t) = -\tanh\left[\left(\frac{y - y_c}{\delta}\right)\cos(\omega t) - \left(\frac{x - x_c}{\delta}\right)\sin(\omega t)\right], \tag{36}$$

where $\omega = V(r)/r$ is the angular velocity and $\delta = 0.05$. The experimental setting is that of Nair *et al.* (1999a); Zerroukat *et al.* (2002). In particular, the domain of integration is $\Omega = [0, 10] \times [0, 10]$ with a 129×129 grid. The time step is $\Delta t = 0.3125$ and a total of 16 time steps is performed. Numerical reference solutions can be found in Zerroukat *et al.* (2002) for the standard bicubic and several conservative SL methods. The corresponding results for the newly proposed advection scheme can be found in Figure 3. It turns out that the rms values of the newly proposed advection scheme are about the same size as those reported by Zerroukat *et al.* (2002).

Table I. Convergence of l_2-errors as a function of $\Delta x = 1/M$ for uniform advection with $U = 1$ of a sine wave on a periodic domain $\Omega = [0, 1]$ with $\Delta t = 0.12\Delta x/U$ and 20 time steps.

M	8	16	32	64	128	256	512
l_2	0.549E-02	0.254E-03	0.143E-4	0.872E-6	0.541E-07	0.337E-08	0.211E-09

DOI: 10.1002/qj

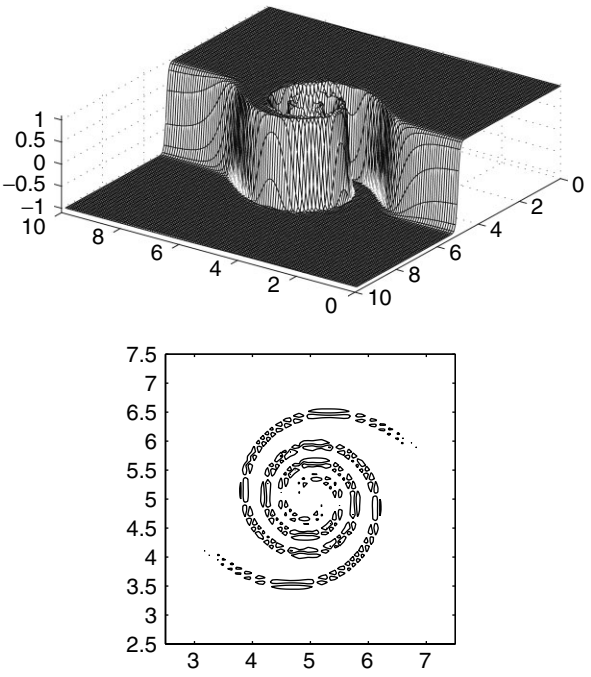

Figure 3. Cyclogenesis problem. Top panel: numerical solution at time $t = 5$. Bottom panel: error (analytic minus numerical) with contour minimum -0.627 and contour interval 0.418; error measures, as defined in Zerroukat *et al.* (2002), $\text{rms}_1 = 0.081439$, $\text{rms}_2 = 0.037703$, and $\text{pdm} = 1.76259 \times 10^{-12}$.

6.4. Spherical advection: Solid body rotation

Solid body rotation is a commonly used experiment to test an advection scheme over the sphere. The experimental setting of Nair and Machenhauer (2002); Nair *et al.* (2002); Nair *et al.* (2003); Zerroukat *et al.* (2004) was applied. The initial density is the cosine bell,

$$\rho_0(\lambda, \theta) = \begin{cases} 1/2\,[1 + \cos(\pi r/R)], & r \le R, \\ 0, & r > R, \end{cases} \qquad (37)$$

where $R = 7\pi/64$,

$$r = \cos^{-1}\left[\sin\theta + \cos\theta\,\cos(\lambda - \lambda_c)\right], \qquad (38)$$

and $\lambda_c = 3\pi/2$. The bell is advected by a time-invariant velocity field

$$u = \cos\alpha\,\cos\theta + \sin\alpha\,\cos\lambda\,\sin\theta, \qquad (39)$$

$$v = -\sin\alpha\,\sin\lambda, \qquad (40)$$

where (u, v) are the velocity components in λ and θ direction, respectively, and α is the angle between the axis of solid body rotation and the polar axis of the sphere.

Experiments are conducted for $\alpha = 0$, $\alpha = \pi/2$, and $\alpha = \pi/2 - 0.05$. Analytic trajectories are used and Δt is chosen such that 256 time steps correspond to a complete revolution around the globe (the radius of the sphere is set equal to one). Accuracy is measured as relative errors in the l_1, l_2, and l_∞ norms (as defined, for example, in Zerroukat *et al.* (2004)). Results are reported in Table II

Table II. Comparison of error norms for solid body rotation with three different values of α t after one complete revolution using 256 time steps over a 128×64 grid. The meridional Courant number is $C_\theta = 0.5$.

α	0	$\pi/2$	$\pi/2 - 0.05$
l_1	0.0492	0.0591	0.0627
l_2	0.0336	0.0393	0.0397
l_∞	0.0280	0.0367	0.0374

for a 128×64 grid (i.e. $J = 64$). It turns out that the relative errors of the newly proposed advection scheme are about the same size as those reported by Zerroukat *et al.* (2004).

Note that (31) may lead to a non-uniform distribution of particle masses near the polar cap regions for meridional Courant numbers $C_\theta > 1$. This can imply a loss of accuracy if a 'heavy' extra-polar particle moves into a polar cap region. This was verified for 72, 36 and 18, respectively, time steps per complete revolution (implying a meridional Courant number of $C_\theta = 1.78$, $C_\theta = 3.56$, and $C_\theta = 7.12$, respectively). It was found that the accuracy is improved by applying a smoothing operator along lines of constant θ near the polar caps, e.g.

$$\rho^{n+1} = \left[1 - \left(\frac{\gamma}{\cos\theta}\right)^6 \frac{\partial^6}{\partial\lambda^6}\right]^{-1} \rho_*^{n+1}, \qquad (41)$$

$\gamma \ll \pi/J$, $J = 64$. Here ρ_*^{n+1} denotes the density approximation obtained from (30). The filter (41) is mass conserving and acts similarly to hyper-viscosity. The disadvantage of this simple filter is that $\rho^{n+1} \neq \rho^n$ under zero advection.

Results for $\gamma = 0$ and $\gamma = \pi/192$, respectively, and 72, 36 and 18 time steps, respectively, are reported in Table III. It is evident that filtering by (41) improves the results significantly. Corresponding results for standard advection schemes can be found in Nair and Machenhauer (2002) for the case of 72 time steps per complete revolution. It turns out that the relative errors of the newly proposed advection scheme with $\gamma = \pi/(3J)$ are slightly

Table III. Comparison of error norms for solid body rotation with $\alpha = \pi/2$ for different values of the smoothing parameter γ in (41) after one complete revolution over a 128×64 grid (i.e., $J = 64$). Panel (a): Complete revolution using 72 time step. The meridional Courant number is $C_\theta = 1.78$. Panel (b): Complete revolution using 36 time step. The meridional Courant number is $C_\theta = 3.56$. Panel (c): Complete revolution using 18 time step. The meridional Courant number is $C_\theta = 7.12$.

	(a) 72 time steps		(b) 36 time steps		(c) 18 time steps	
γ	0	$\pi/(3J)$	0	$\pi/(3J)$	0	$\pi/(3J)$
l_1	0.0491	0.0283	2.3264	0.0222	2.3217	0.0143
l_2	0.0468	0.0168	1.5124	0.0137	1.5126	0.0105
l_∞	0.0723	0.0122	1.1383	0.0151	1.0764	0.0143

DOI: 10.1002/qj

smaller than as those reported by Nair and Machenhauer (2002).

6.5. Spherical advection: Smooth deformational flow

To further evaluate the accuracy of the advection scheme in spherical geometry, the idealized vortex problem of Doswell (1984) is considered. The flow field is deformational and an analytic solution is available (see Nair *et al.*, 1999b; Nair and Machenhauer, 2002 for details).

The mathematical formulation can be summarized as follows. Let (λ', θ') be a rotated coordinate system with the north pole at $(\pi + 0.025, \pi/2.2)$ with respect to the regular spherical coordinates. We consider rotations of the (λ', θ') coordinate system with an angular velocity ω, i.e.

$$\frac{d\lambda'}{dt} = \omega, \qquad \frac{d\theta'}{dt} = 0, \tag{42}$$

where

$$\omega(\theta') = \frac{3\sqrt{3}\,\mathrm{sech}^2(3\cos\theta')\tanh(3\cos\theta')}{6\cos\theta'}. \tag{43}$$

An analytic solution to the continuity equation (1) in (λ', θ') coordinates is provided by

$$\rho(\lambda', \theta', t) = 1 - \tanh\left[\frac{3\cos\theta'}{5}\sin(\lambda' - \omega(\theta')\,t)\right]. \tag{44}$$

Simulations are performed using a 128×64 grid and a step size of $\Delta t = 0.05$. The filter (41) is not applied. The exact solution (evaluated over the given grid) and its numerical approximation at times $t = 3$ and $t = 6$ are displayed in Figure 4. The relative l_1, l_2 and l_∞ errors (as defined in Zerroukat *et al.*, 2004) can be found in Table IV. These errors are slightly larger than the ones reported in Nair and Machenhauer (2002) and Zerroukat *et al.* (2004). It can also be concluded from Figure 4 that the numerical solution at $t = 3$ is somewhat lagging behind the analytic one while, at $t = 6$, the difference between the numerical and analytic solution is very large near the pole.

6.6. Rotating shallow-water equations in planar geometry

To demonstrate the behaviour of the new advection scheme under a time-dependent and compressible velocity field, we consider the shallow-water equations (SWEs)

Table IV. Comparison of error norms at different times t for spherical polar vortex problem. Computations are performed with a step size of $\Delta t = 1/20$ and a 128×64 grid.

t	3	6
l_1	0.0019	0.0055
l_2	0.0062	0.0172
l_∞	0.0324	0.0792

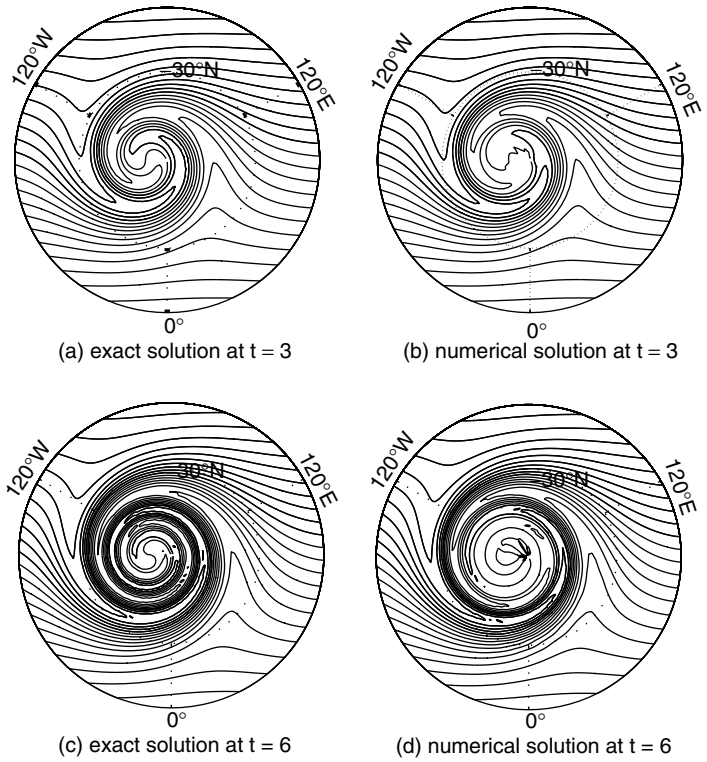

Figure 4. Results of a polar vortex simulation over the sphere. The exact solution and its numerical approximation at time $t = 3$ can be found in panels (a) and (b), respectively. Contours plotted between 0.5 and 1.5 with contour interval 0.05. Panels (c) and (d) display the same results for time $t = 6$.

DOI: 10.1002/qj

on an f-plane (Durran, 1998; Salmon, 1999):

$$\frac{Du}{Dt} = +fv - g\mu_x, \tag{45}$$

$$\frac{Dv}{Dt} = -fu - g\mu_y, \tag{46}$$

$$\frac{D\mu}{Dt} = -\mu\,(u_x + v_y). \tag{47}$$

Here $\mu = \mu\,(x, y, t)$ is the fluid depth, g is the gravitational constant, and f is twice the (constant) angular velocity of the reference plane.

Let H denote the maximum value of μ over the whole fluid domain. The fluid depth perturbation $\tilde{\mu} = \mu - H$ is also introduced. The perturbation satisfies the continuity equation

$$\frac{D\tilde{\mu}}{Dt} = -\tilde{\mu}\,(u_x + v_y) \tag{48}$$

which is solved numerically using the newly proposed scheme. The overall time stepping procedure is given by the semi-Lagrangian Störmer–Verlet (SLSV) method with only equation (5.7) from Reich (2006) being replaced by the following steps:

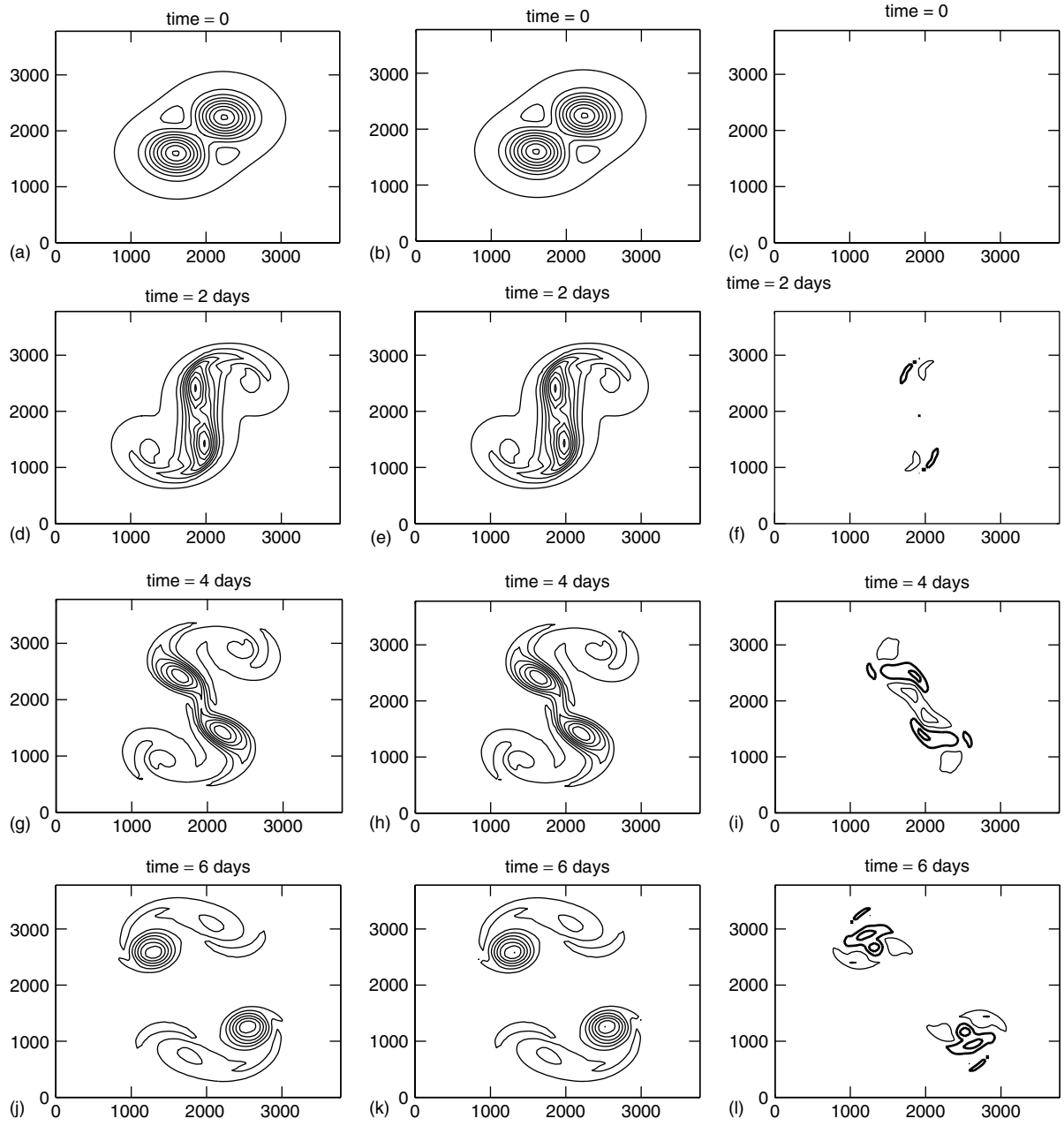

Figure 5. Left panels: Computed time evolution, from initial time to $t = 6$ days, of PV over the domain $(x, y) \in [0, 3840\,\text{km}] \times [0, 3840\,\text{km}]$ using the semi-Lagrangian Störmer–Verlet (SLSV) method and the remapped particle-mesh advection scheme with cubic splines. The time step is $\Delta t = 20\,\text{min}$. Contours plotted between $6.4 \times 10^{-8}\,\text{m}^{-1}\text{s}^{-1}$ and $2.2 \times 10^{-7}\,\text{m}^{-1}\text{s}^{-1}$ with contour interval $1.56 \times 10^{-8}\,\text{m}^{-1}\text{s}^{-1}$. Middle panels: Time evolution of PV as obtained from a semi-implicit semi-Lagrangian (SISL) method. Right panels: Differences (semi-Lagrangian Störmer–Verlet minus semi-implicit semi-Lagrangian) at corresponding times are plotted with a 10 times smaller contour interval, where thin (thick) lines are positive (negative) contours.

DOI: 10.1002/qj

(i)

$$\mu^{n+1/2-\varepsilon} = \mu^n - \frac{\Delta t H}{2}\left[u_x + v_y\right]^{n+1/2-\varepsilon}.$$

(ii) Solve (48) over a full time step using the newly proposed remapped particle-mesh advection scheme with velocities $(u^{n+1/2-\varepsilon}, v^{n+1/2-\varepsilon})$ and initial fluid depth perturbation $\tilde{\mu}^{n+1/2-\varepsilon} = \mu^{n+1/2-\varepsilon} - H$. Denote the resulting fluid depth by $\mu^{n+1/2+\varepsilon} = \tilde{\mu}^{n+1/2+\varepsilon} + H$. We implemented the remapped particle-mesh advection scheme with linear and cubic splines, respectively.

(iii)

$$\mu^{n+1} = \mu^{n+1/2+\varepsilon} - \frac{\Delta t H}{2}\left[u_x + v_y\right]^{n+1/2+\varepsilon}.$$

The SLSV method has been implemented using the standard C-grid (Durran, 1998) over a double periodic domain with $L_x = L_y = 3840$ km (see Staniforth *et al.*, 2006 for details). The grid size is $\Delta x = \Delta y = 60$ km. The time step is $\Delta t = 20$ min and the value of f corresponds to an f-plane at 45^o latitude. The reference height of the fluid is set to $H = 9665$ m. The Rossby

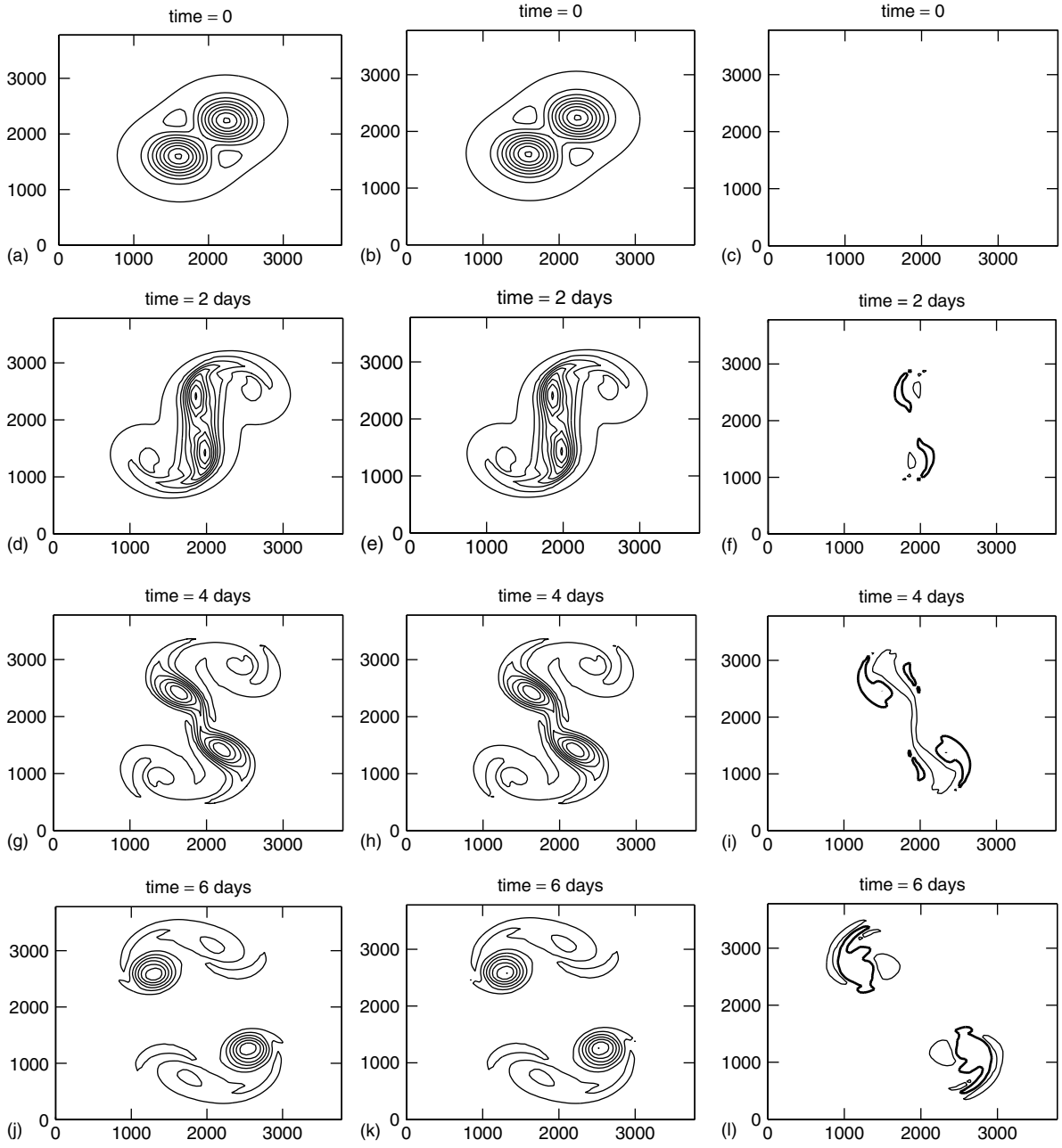

Figure 6. Left panels: Computed time evolution, from initial time to $t = 6$ days, of PV over the domain $(x, y) \in [0, 3840\,\text{km}] \times [0, 3840\,\text{km}]$ using the semi-Lagrangian Störmer-Verlet (SLSV) method and the remapped particle-mesh advection scheme with linear splines. The time step is $\Delta t = 20$ min. Contours plotted between $6.4 \times 10^{-8}\,\text{m}^{-1}\text{s}^{-1}$ and $2.2 \times 10^{-7}\,\text{m}^{-1}\text{s}^{-1}$ with contour interval $1.56 \times 10^{-8}\,\text{m}^{-1}\text{s}^{-1}$. Middle panels: PV evolution as obtained from a semi-implicit semi-Lagrangian (SISL) method. Right panels: Differences (semi-Lagrangian Störmer-Verlet minus semi implicit semi-Lagrangian) at corresponding times are plotted with a 10 times smaller contour interval, where thin (thick) lines are positive (negative) contours.

DOI: 10.1002/qj

radius of deformation is $L_R \approx 3000$ km. Initial conditions are chosen as in Staniforth *et al.* (2006); Reich (2006) and results are displayed in an identical format for direct comparison.

To assess the new discretization, results are compared to those from a two-time-level semi-implicit semi-Lagrangian (SISL) method with a standard bicubic interpolation approach to semi-Lagrangian advection (see, e.g. McDonald and Bates, 1987; Temperton and Staniforth, 1987). The resulting nonlinear equations are iterated to convergence. It is apparent from Figures 5 and 6 that the SLSV and SISL simulations yield similar results in terms of potential vorticity advection. Furthermore, the results displayed in Figures 5 and 6 are nearly identical to those displayed in Figure 6.1 of Reich (2006). The good behaviour of the linear spline implementation of the remapped particle-mesh advection scheme is rather surprising and has been confirmed for other simulations such as a shear flow instability.

7. Summary and outlook

A computationally efficient and mass conserving forward trajectory semi-Lagrangian approach has been proposed for the solution of the continuity equation (1). At every time step a 'mass' is assigned to each grid point which is then advected downstream to a (Lagrangian) position. The gridded density at the next time step is obtained by evaluating a bicubic spline representation with the advected masses as weights. The main computational cost is given by the need to invert tridiagonal linear systems in (20). Computationally efficient iterative or direct solvers are available. We also proposed an extension of the advection scheme to spherical geometry. A further generalization to 3D would be straightforward. Numerical experiments show that the new advection scheme achieves accuracy comparable to standard non-conserving and published conserving SL schemes. The main drawbacks of the proposed approach are that higher order splines do not lead to monotonicity preserving schemes and that conservation of mass is not strictly local (in the sense of finite-volume methods).

We note that the proposed advection scheme can be used to advect momenta according to

$$\frac{D}{Dt}(\rho \mathbf{u}) = -(\rho \mathbf{u}) \nabla \cdot \mathbf{u}. \tag{49}$$

This possibility is particularly attractive in the context of the newly proposed semi-Lagrangian Störmer–Verlet (SLSV) scheme (Reich, 2006).

Acknowledgements

We would like to thank Nigel Wood for discussions and comments on earlier drafts of this manuscript.

References

Doswell CA. 1984. A kinematic analysis of frontogenesis associated with a nondivergent vortex. *J. Atmos. Sci.* **41**: 1242–1248.

Durran DR. 1998. *Numerical Methods for Wave Equations in Geophysical Fluid Dynamics*. Springer-Verlag: New York.

Frank J, Gottwald G, Reich S. 2002. The Hamiltonian particle-mesh method method. In *Meshfree methods for partial differential equations*, Griebel M, Schweitzer MA (eds). Springer-Verlag: Heidelberg; Pp. 131–142; *Lect. Notes Comput. Sci. Eng.* **26**.

Frank J, Reich S. 2004. The Hamiltonian particle-mesh method for the spherical shallow water equations. *Atmos. Sci. Lett.* **5**: 89–95.

Gingold RA, Monoghan JJ. 1977. Smoothed particle hydrodynamics: Theory and applications to non-spherical stars. *Mon. Not. R. Astr. Soc.* **181**: 375–389.

Harlow F. 1964. The particle-in-cell computing methods for fluid dynamics. *Methods Comput. Phys.* **3**: 319–343.

Kaas E, Guldberg A, Lopez P. 1997. A Lagrangian advection scheme using tracer points. In *Numerical methods in atmospheric and ocean modelling. The André J. Robert memorial volume*, Lin C, Laprise R, Ritchie H (eds). Canadian Meteorological and Oceanographic Society: Ottawa, Canada; Pp. 171–194.

Laprise JPR, Plante A. 1995. A class of semi-Lagrangian integrated-mass (SLIM) numerical transport algorithms. *Mon. Weather Rev.* **123**: 553–565.

Lucy LB. 1977. A numerical approach to the testing of the fission hypothesis. *Astron. J.* **82**: 1013–1024.

McDonald A, Bates JR. 1987. Improving the estimate of the departure point in a two-time level semi-Lagrangian and semi-implicit scheme. *Mon. Weather Rev.* **115**: 737–739.

Nair RD, Coté J, Staniforth A. 1999a. Monotonic cascade interpolation for semi-Lagrangian advection. *Q. J. R. Meteorol. Soc.* **125**: 197–212.

Nair RD, Coté J, Staniforth A. 1999b. Cascade interpolation for semi-Lagrangian advection over the sphere. *Q. J. R. Meteorol. Soc.* **125**: 1445–1468.

Nair RD, Machenhauer B. 2002. The mass-conservative cell-integrated semi-Lagrangian advection scheme on the sphere. *Mon. Weather Rev.* **130**: 649–667.

Nair RD, Scroggs JS, Semazzi FHM. 2002. Efficient conservative global transport schemes for climate and atmospheric chemistry models. *Mon. Weather Rev.* **130**: 2059–2073.

Nair RD, Scroggs JS, Semazzi FHM. 2003. A forward-trajectory global semi-Lagrangian transport scheme. *J. Comp. Phys.* **190**: 275–294.

Purser RJ, Leslie LM. 1991. An efficient interpolation procedure for high-order three-dimensional semi-Lagrangian models. *Mon. Weather Rev.* **119**: 2492–2498.

Reich S. 2006. Linearly implicit time stepping methods for numerical weather prediction. *BIT* **46**: 607–616.

Robert A. 1982. A semi-Lagrangian and semi-implicit numerical integration scheme for the primitive meteorological equations. *J. Meteorol. Soc. Jpn.* **60**: 319–325.

Salmon R. 1999. *Lectures on geophysical fluid dynamics*. Oxford University Press: Oxford.

Spotz WF, Taylor MA, Swarztrauber PN. 1998. Fast shallow-water equation solvers in latitude-longitude coordinates. *J. Comp. Phys.* **145**: 432–444.

Staniforth A, Coté J. 1991. Semi-Lagrangian integration schemes for atmospheric models – A review. *Mon. Weather Rev.* **119**: 2206–2223.

Staniforth A, Wood N, Reich S. 2006. A time-staggered semi-Lagrangian discretization of the rotating shallow-water equations. *Q. J. R. Meteorol. Soc.* (in press).

Temperton C, Staniforth A. 1987. An efficient two-time-level semi-Lagrangian semi-implicit integration scheme. *Q. J. R. Meteorol. Soc.* **113**: 1025–1039.

Zerroukat M, Wood N, Staniforth A. 2002. SLICE: A semi-Lagrangian inherently conserving and efficient scheme for transport problems. *Q. J. R. Meteorol. Soc.* **128**: 801–820.

Zerroukat M, Wood N, Staniforth A. 2004. SLICE-S: A semi-Lagrangian inherently conserving and efficient scheme for transport problems on the sphere. *Q. J. R. Meteorol. Soc.* **130**: 2649–2664.

Zerroukat M, Wood N, Staniforth A. 2006a. The parabolic sline method (PSM) for conservative transport problems. *Int. J. Numer. Meth. Fluids* **51**: 1297–1318.

Zerroukat M, Wood N, Staniforth A. 2006b. Application of the parabolic spline method (PSM) to a multi-dimensional conservative semi-Lagrangian transport scheme (SLICE). *J. Comp. Phys.* In press.

DOI: 10.1002/qj